NJC

PAPER

Cite this: *New J. Chem.*, 2022, **46**, 15495

A carbon nanowire-promoted Cu_2O/TiO_2 nanocomposite for enhanced photoelectrochemical performance

Kassam Ahmed,[a] Yuyin Wang,[b] Yang Bai,[b] Karthikeyan Sekar *[c] and Wei Li *[b]

Received 23rd June 2022,
Accepted 11th July 2022

DOI: 10.1039/d2nj03116g

rsc.li/njc

The use of semiconductors as photoelectrochemical electrodes and photocatalysts has been studied extensively over the last few decades; however, it is challenging to design one single material meeting a wide range of requirements for applications such as photostability, wide light absorbance and earth abundance. In this study, we started with earth-abundant materials, namely TiO_2, Cu_2O and carbon, to design a nanocomposite with TiO_2 nanofibers (NFs) and Cu_2O nanocubes (NCs) connected by carbon nanowires (NWs). The nanocomposite ($C/TiO_2/Cu_2O$) demonstrated excellent photo(electro)activity under simulated visible light as well as enhanced durability. Morphologies imaged by electron microscopes showed that TiO_2 NFs and Cu_2O NCs were well connected, while thin and long carbon NWs were present throughout the samples and connected the NFs and NCs to form a compact composite. Electrochemical analysis revealed that the band alignment between TiO_2 and Cu_2O was typical for a type-II heterojunction, which is favourable for the separation of photogenerated charge carriers. Moreover, carbon NWs act as bridges, thus facilitating more efficient charge transfer. Overall, this research showed the design and preparation of a nanostructured composite with improved charge transfer and photostability for solar photoelectrochemical applications.

1. Introduction

Technologies based on photon and semiconductor interactions, *e.g.* photoelectrochemical and photocatalysis water splitting, have become attractive research areas in recent decades because they can offer a sustainable roadmap towards clean fuels and the environment. An important factor for advancing the research is to obtain catalytic/electrode materials with suitable properties, such as wide light absorbance, photostability, high efficiency, environment friendliness and earth abundance. An extensive range of materials have been studied over the last few decades,[1–10] but each has its own limitations.[11–15]

Titanium dioxide (TiO_2) is a well-known stable n-type semiconductor used over the last few decades with a large band gap of 3.2 eV;[11] thus, it is mainly active in the ultraviolet (UV) region, which is only 4% of the solar spectrum. Efforts have been devoted to expanding the spectral response of TiO_2 in the visible light region using various band engineering methods, such as surface modification, metal doping, creating heterojunction, co-catalyst loading and coupling with narrow band gap semiconductors.[16]

A highly attractive narrow band gap semiconductor, Cu_2O, is found in abundant, low-cost and non-toxic p-type semiconductor with a band gap between 2.0 and 2.2 eV.[17] However, Cu_2O is prone to photocorrosion, which is attributed to the oxidation and reduction potential of Cu_2O lying within the band gap.[18]

TiO_2–Cu_2O as a binary heterojunction/composite has demonstrated synergistic photoelectrochemical and photocatalytic performance based on efficiency and stability.[19] However, there are inevitable defects or poor connections at the interface between the two different components, which act as charge carrier sinks and hinder efficient charge carrier migration. A strategy to improve the interface and provide better connections between the two different components is highly desirable to fully unleash the synergy between TiO_2 and Cu_2O, thus providing an ideal catalyst for photoelectrochemical and photocatalytic applications.

There are attempts to utilise carbon nanomaterials in composite photoelectrochemical electrode materials and photocatalysts as charge transfer promoters and structure stabilisers. For example, carbon nanowires (NWs) are known to have excellent mechanical and electron transport properties.[20]

In addition to the physical and chemical properties of TiO_2 and Cu_2O, their structural properties (*e.g.* morphology, surface

[a] *School of Engineering and Applied Science, Aston University, Birmingham B4 7ET, UK*
[b] *Institute for Materials and Processes, School of Engineering, University of Edinburgh, Mayfield Road, Edinburgh EH9 3JL, UK. E-mail: wei.li@ed.ac.uk*
[c] *Department of Chemistry, SRM Institute of Science and Technology, Kattankulathur, Tamil Nadu, India. E-mail: karthik.keyan02@gmail.com*

area and crystallinity) also play vital roles in their photoelectrochemical and photocatalytic properties. In our previous study, it is already revealed that high crystalline TiO_2 nanofibers (NFs) and Cu_2O nanocubes (NCs) can offer optimised charge transfer efficiency and photostability compared to other structures.[19,21–23]

In this study, we designed a nanocomposite with TiO_2 NFs and Cu_2O NCs, which was further connected and enhanced by carbon NWs. The synthesis procedure was simple and required inexpensive solvents and operating conditions. The photoelectrochemical (PEC) performance of the ternary C-NW/TiO_2 NF/Cu_2O composite showed improved charge carrier separation, superior PEC activity and enhanced stability.

2. Experimental

2.1. Synthesis of C-NW/TiO_2 NF

A single crystalline 1D TiO_2 NF was fabricated as described in our previous study *via* topotactic transformation by ion-exchange and dehydration.[22] Subsequent C-NW/TiO_2 NF was prepared by a hydrothermal synthesis using gelatine as the carbon precursor as it is a cheap polymer obtained from animal skin, bones and tissues.[24] It is known to have strong coating interactions with metal nanoparticles.[25] Gelatine was dissolved in a mixture of TiO_2 NFs in 20 ml water and stirred at 40 °C. The sample was placed in a stainless-steel autoclave and heated at 250 °C for 4 h. After the hydrothermal treatment, the sample was centrifugated at 7000 rpm for 10 min with several washes of water and dried in the oven. Gelatine is abundant in amino and carboxyl groups, so it can be hydrothermally treated with only pure water. Hence, it is an inexpensive water-soluble polymer. An advantage of this procedure is that no strong acid or surface passivation reagent or post-treatment is needed to fabricate C-NW/TiO_2 NFs.[26]

2.2. Synthesis of C-NW/TiO_2 NF/Cu_2O

C-NW/TiO_2 NF/Cu_2O was synthesised by solution phase chemistry under ambient conditions, as described previously.[16] The TiO_2 to Cu_2O ratio was targeted at 1 : 1 by controlling the dosages of corresponding precursors in the synthesis process. In a typical process, PEG was ultrasonicated in 100 ml of water for 30 min. C-NW/TiO_2 NF was mixed with 0.2 M $CuCl_2$ and 0.01 M PEG-600 before ultrasonication for 10 min. This mixture was then heated to 50 °C, forming a blue solution. 2 M NaOH was poured into the blue solution and 0.2 M $N_2H_4 \cdot H_2O$ was added dropwise in the stirred mixture to generate Cu(I) ions and further heated for 10 min. The resulting mixture was purged in N_2 to form C-NW/TiO_2 NF/Cu_2O, followed by centrifugation at 7000 rpm with several washes with H_2O and ethanol to remove any residual PEG.

2.3. Characterisation methods

TEM images were taken at 200 kV on a JEM-2100Plus microscope (Warwick University, UK). Samples were prepared by ultrasonication and drop-casted on a Cu grid coated with a carbon film. Powder X-ray diffraction (XRD) was operated on a Bruker-AXS D8 ADVANCE diffractometer at 40 kV, 40 mA and Cu Kα radiation (λ = 0.15418 nm) between 2θ 10 and 80° in 0.02° steps. Brunauer–Emmett–Teller (BET) surface areas were calculated at 77 K by N_2 physisorption using a Quantachrome NOVA 4000e porosimeter on degassed samples at 120 °C for 4 h. Diffuse reflectance UV-Vis Spectra (DRUVS) were recorded on a Thermo Scientific Evo220 Spectrometer using KBr as a standard in an absorbance range between 200 and 700 nm. The ratio of TiO_2 to Cu_2O in TiO_2 NF/Cu_2O and C-NW/TiO_2 NF/Cu_2O samples was quantified by ICP-OES (Optima2000DV, USA).

2.4. Photoelectrochemical methods

A homogenous colloid was formed within 30 min of sonication of the as-prepared samples (5 mg), and Nafion (10 μL, 5 wt%) was dispersed in a water/ethanol mixture (1 ml, 3 : 1 v/v). 5 μL colloid was deposited on a glassy carbon electrode (3 mm dia.) used as the working electrode. A Pt wire was used as the counter electrode, and Hg/Hg_2SO_4 was used as the reference electrode in a three-electrode photoelectrochemical cell. The electrolyte (0.5 M Na_2SO_4) was purged in N_2 for 30 min. A 200 W Hg–Xe arc lamp (Oriel Instruments 66002, with UV cutoff filter, λ > 420 nm) was used as the light source. The light intensity was adjusted and kept at 100 mW cm^{-2} for all experiments. Measurements were performed using Autolab potentiostat with Nova software. Mott–Schottky plots were recorded under DC polarisation at a potential range of −1 to 0 V with a potential step of 10 mV at a frequency of 1000 Hz. Nyquist plots were recorded under an AC signal of 10 mV at a frequency range of 100 kHz–0.1 Hz.

3. Results and discussion

TEM and SEM images in Fig. 1 show the morphology and size of the individual components and C-NW/TiO_2 NF/Cu_2O as a

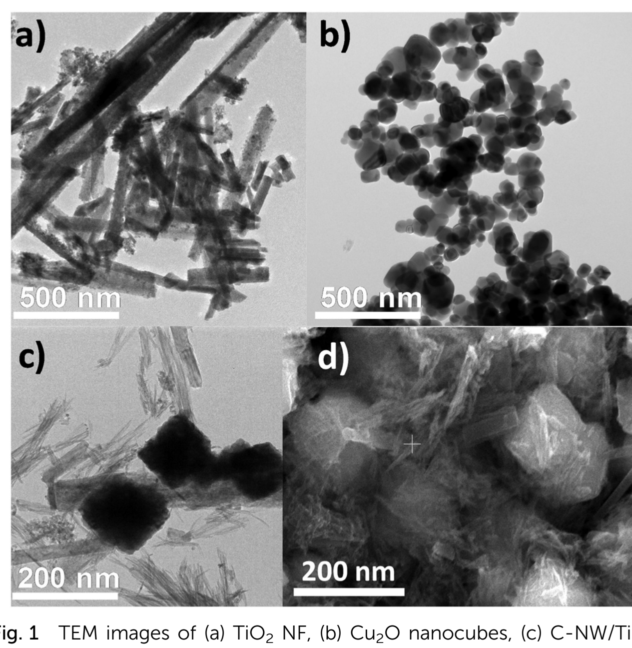

Fig. 1 TEM images of (a) TiO_2 NF, (b) Cu_2O nanocubes, (c) C-NW/TiO_2 NF/Cu_2O, and (d) SEM images of C-NW/TiO_2 NF/Cu_2O.

nanocomposite. Fig. 1a demonstrates the 1D TiO_2 NF with lengths between 500 nm and 5 μm and diameters between 100 and 200 nm. Fig. 1b illustrates the Cu_2O nanocubes with sizes ranging between 150 and 250 nm. After the hydrothermal synthesis, amino acids were carbonised to form carbon NWs, and thus the ternary Cu_2O, C-NW and TiO_2 nanocomposite was formed, as shown in Fig. 1c and d. In these two images, cubic Cu_2O, TiO_2 NF and C-NW were all clearly visible. TiO_2 NFs were intimately in contact with Cu_2O nanocubes, with C-NWs occupying the spaces and further promoting the Cu_2O–TiO_2 connections.

XRD patterns confirmed the characteristics of Cu_2O and TiO_2 peaks in Fig. 2a, indicating that the heterojunction nanocomposite consists of Cu_2O and TiO_2, which is in good agreement with the TEM and SEM images. The diffraction peaks for TiO_2 NF were well defined and corresponded to the crystal planes of (101), (004), (200), (105), (211) and (204) at $2\theta = 25.3°$, 37.8°, 48.0°, 53.8°, 55.4° and 62.5°, respectively, which confirmed anatase TiO_2 NF (tetragonal, JCPDS 21-1272).[27] The XRD patterns illustrated the formation of crystalline Cu_2O by 2θ peaks at 29.6°, 36.4°, 42.3°, 61.4°, 73.5° and 77.4°, which are associated with characteristic (110), (111), (200), (220), (311), and (222) peaks of Cu_2O, respectively (cubic, JCPDS 73-0687).[28] The ratio of TiO_2 to Cu_2O in TiO_2 NF/Cu_2O and C-NW/TiO_2 NF/Cu_2O samples was quantified as 0.9 : 1 by ICP-OES. There were weak traces of CuO in both Cu_2O and TiO_2 NF/Cu_2O, which is in agreement with JCPDS 45-0937[29] but not observed in the C-NW/TiO_2 NF/Cu_2O sample. There is a weak but a broad pattern at 25°, suggesting either a low concentration of C-NWs or the amorphous carbon.

The carbon content in C-NW/TiO_2 NF/Cu_2O was investigated by thermogravimetric analysis (TGA), as shown in Fig. 2b. There are three significant weight losses at 100 °C, 200 °C and 400 °C, respectively. The initial loss for the samples at 100 °C was due to the adsorbed moisture (2.1%), while the 2.9% weight loss until 200 °C was attributed to the removal of residual PEG, which was the structuring agent used to fabricate Cu_2O nanocubes. The weight loss above 200 °C was 4.3%, which accounted for the total loss of C-NWs in the heterojunction. Different C-NW contents (*i.e.*, in the range from 2% to 10%) were prepared. Within this range, there was no clear difference in various photoelectrochemical performances. This 4.3% sample was presented as a representative. Fig. 2c illustrates the nature of carbon in C-NW/TiO_2 NF/Cu_2O using Raman spectroscopy. The Raman spectrum shows two peaks of 1370 cm^{-1} and 1593 cm^{-1} for the D and G bands, respectively, which is characteristic of amorphous carbon.

Surface areas varied between the different samples (Fig. 2d), with Cu_2O nanocubes having the lowest BET surface area of 22.9 $m^2\ g^{-1}$. TiO_2 NF exhibited the highest BET surface area of 93.5 $m^2\ g^{-1}$. Binary TiO_2 NF/Cu_2O had a surface area of 53.8 $m^2\ g^{-1}$ reasonably between the two individual components. C-NW/TiO_2 NF/Cu_2O had a higher BET surface area than TiO_2 NF/Cu_2O, which was due to the integration of C-NWs as it has a high surface area. This may have further implications for photoelectrochemical performance because C-NWs may act as an electron anchor by improving electron mobility and transportation in the heterojunction.[30,31]

The optical properties of different samples were analysed and presented in Fig. 3, whereby the absorbance spectra ranged from 200 to 600 nm (Fig. 3a), consistent with previously reported.[32]

The optical band gaps E_{BG} were calculated from the Tauc plots (Fig. 3b) using eqn (1).

$$\alpha h\nu = C(h\nu - E_{BG})^n \quad (1)$$

where C is the proportionality constant and 'α' is the absorption coefficient determined from the Kubelka–Munk formula (eqn (2)).

$$\alpha = \frac{(1-R)^2}{2R} \quad (2)$$

The direct band gaps of TiO_2 NF, Cu_2O, TiO_2 NF/Cu_2O and C-NW/TiO_2 NF/Cu_2O were 3.28, 2.36, 2.38 and 2.21 eV, respectively, as presented in Table 1. The tested samples containing

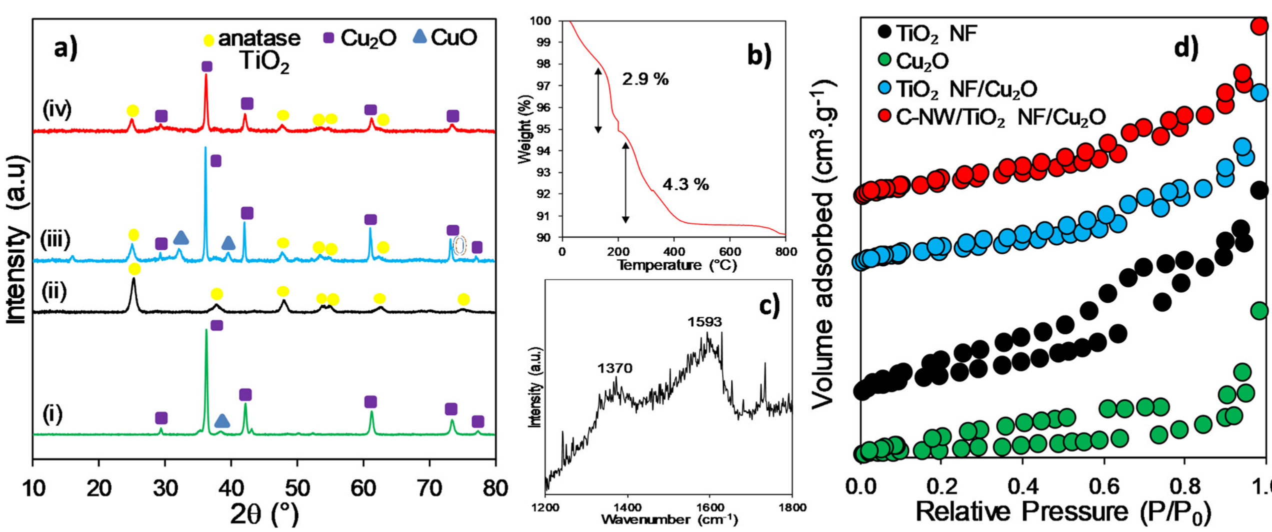

Fig. 2 (a) XRD patterns of (i) Cu_2O, (ii) TiO_2 NF, (iii) TiO_2 NF/Cu_2O and (iv) C-NW/TiO_2 NF/Cu_2O. (b) TGA and (c) Raman spectrum of C-NW/TiO_2 NF/Cu_2O. (d) N_2 adsorption–desorption isotherms of TiO_2 NF, Cu_2O nanocubes, TiO_2 NF/Cu_2O, C-NW/TiO_2 NF/Cu_2O.

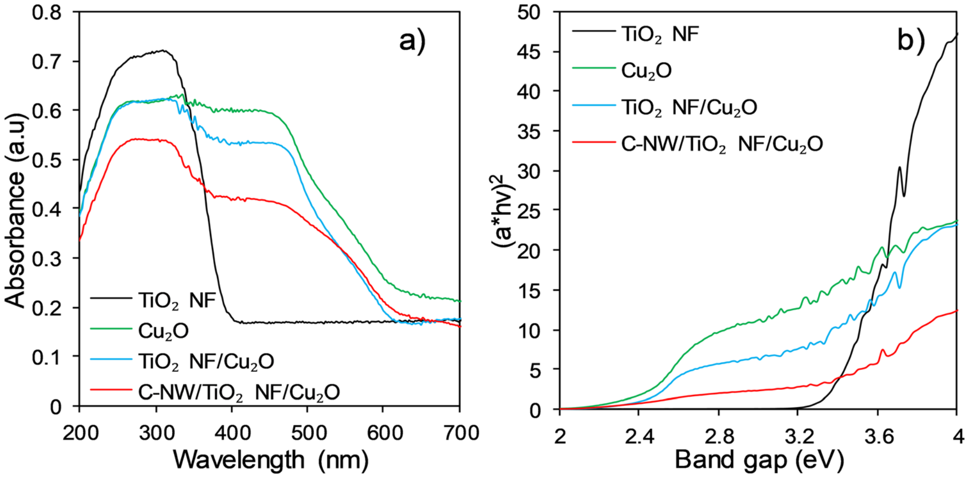

Fig. 3 (a) DRUVS and (b) Tauc plots of TiO_2 NF, Cu_2O, TiO_2 NF/Cu_2O and C-NW/TiO_2 NF/Cu_2O.

Table 1 Photophysical properties of TiO_2 NF, Cu_2O, TiO_2 NF/Cu_2O and C-NW/TiO_2 NF/Cu_2O

Sample	BET surface area[a] (m^2 g^{-1})	Band gap[b] (eV)
TiO_2 NF	93.5	3.28
Cu_2O	22.9	2.36
TiO_2 NF/Cu_2O	53.8	2.38
C-NW/TiO_2 NF/Cu_2O	66.9	2.21

[a] N_2 porosimetry. [b] DRUVS.

Cu_2O absorbed light in the visible region at the wavelength of 650 nm. Two absorbance peaks are present at 300 nm and 480 nm, confirming both components were present in the system, which is in agreement with a previous report.[33] C-NW/TiO_2 NF/Cu_2O showed a red shift to TiO_2 NF/Cu_2O, which indicates C-NWs have strong visible light absorption properties. It may also promote interfacial contact between C-NWs and the two semiconductors.

The effect of C-NW enhancement on the interfacial charge transfer between the TiO_2 NF–Cu_2O heterojunction was investigated using PEC measurements under chopped visible light illumination at 0 V *vs.* RHE. PEC measurements were studied in a three-electrode system, with Pt wire as the counter electrode, Hg/Hg_2SO_4 as the reference electrode, and different samples were drop-casted onto a glassy carbon electrode as the working electrode. Fig. 4a shows C-NW/TiO_2 NF/Cu_2O > TiO_2 NF/Cu_2O > Cu_2O > TiO_2 NF in terms of photoresponse. In order to enable comparison with other reported and relevant TiO_2-based materials, the widely used benchmark P25 TiO_2 was also tested, showing photoresponse similar to TiO_2 NF (data did not show as it overlapped with that of TiO_2 NF), which was consistent with our previous study.[19] The low photocurrent density of TiO_2 NF was attributed to poor visible light response, and Cu_2O had photostability issues during charge transfer. The photocurrent density of C-NW/TiO_2 NF/Cu_2O was approximately 6 times higher than TiO_2 NF/Cu_2O and above the factor of 8 times higher than both Cu_2O and TiO_2 NF. The C-NW promoted the heterojunction nanocomposite produced a higher photocurrent response, indicating more efficient charge transfer, where C-NWs can act as a carrier mobility layer at the TiO_2 NF/Cu_2O interface.[34] Cu_2O was difficult to use in practical applications as it has low photostability; therefore, the impact of C-NWs on catalyst stability (Fig. 4b) was studied. The photocurrent generated by Cu_2O decreased at a faster rate than C-NW/TiO_2/Cu_2O over a time period of 24 hours, which suggests that the addition of TiO_2 NF and C-NWs increased photostability. The advantage of C-NW as a conductive network was more profound when we consider that the samples were dropcasted on a glassy carbon electrode. The sample particles formed a dense layer with the C-NW conductive network embedded, which could not only promote the charge mobility but also enhance the Cu_2O stability.

Bare TiO_2 NF showed a low photocurrent density *vs.* voltage curves (Fig. 4c), but Cu_2O nanocubes exhibited a higher photocurrent density under visible light due to its narrow band gap. With the introduction of the heterojunction nanocomposite, TiO_2 NF/Cu_2O, the photocurrent density increased to 60.3 μA cm^{-2} at 1.23 V *vs.* RHE. The integration of C-NWs yielded a significant increase in the photocurrent density of 139.8 μA cm^{-2}, which was almost 4 times higher than TiO_2 NF. The sharp increase in the photocurrent density indicates high charge transfer and separation efficiency with C-NWs in C-NW/TiO_2 NF/Cu_2O.[35] The results were similar in the chopped photocurrent density *vs.* voltage curve, as shown in Fig. 4d, where C-NW/TiO_2 NF/Cu_2O reached photocurrent densities of 122.4 μA cm^{-2} at −0.3 V *vs.* RHE, which was 2 times higher than TiO_2 NF/Cu_2O.

The interfacial properties of C-NW/TiO_2 NF/Cu_2O were further studied by electrochemical impedance spectroscopy (EIS) in the form of a Nyquist plot. A Nyquist plot was used to investigate the characteristics of the charge transfer process, whereby the semicircle diameter indicates the charge transfer resistance. In Fig. 5a, the semicircle diameter of Cu_2O and TiO_2 NF is slightly larger than that of TiO_2 NF/Cu_2O, which shows they have similar charge transfer resistance. C-NW/TiO_2 NF/Cu_2O exhibited the lowest charge transfer resistance, which is attributed to the integration of C-NWs. This indicates that C-NWs reduced the resistance to charge carrier transport due to

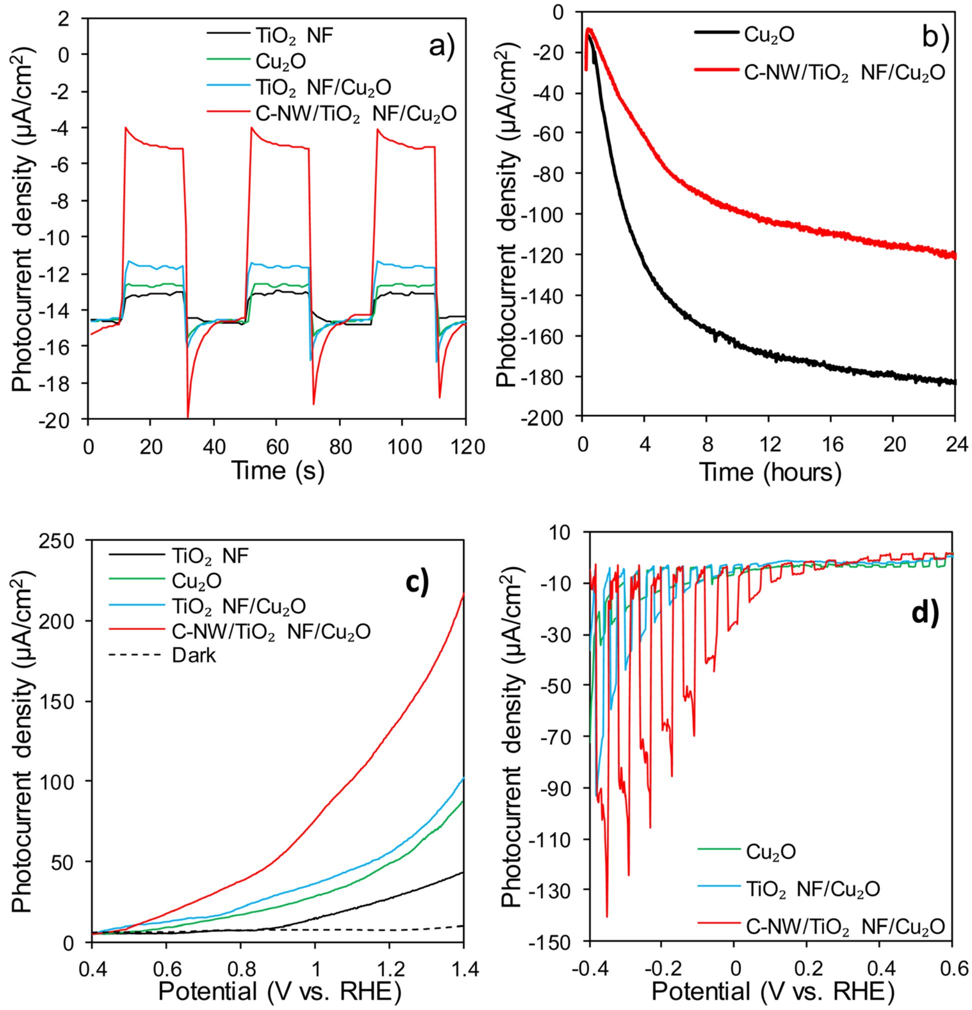

Fig. 4 (a) Transient photocurrent and (b) photostability (0 V *vs.* RHE) of TiO_2 NF, Cu_2O, TiO_2 NF/Cu_2O and C-NW/TiO_2 NF/Cu_2O under visible light irradiation. (c) *I–V* curve and (d) chopped *I–V* curves of TiO_2 NF, Cu_2O, TiO_2 NF/Cu_2O and C-NW/TiO_2 NF/Cu_2O under visible light irradiation at a scan rate of 10 mV s^{-1}, (reaction conditions: 200 W Hg–Xe arc lamp, 0.5 M Na_2SO_4 electrolyte).

the efficient separation of charge carriers in the nanocomposite.[35] Fig. 5b and c show the Mott–Schottky plots of TiO_2 NF, C-NW/TiO_2 NF and Cu_2O, which were utilised to calculate the flat band potential and majority carrier densities of each semiconductor in the heterojunction. The positive and negative slopes are indicative of n-type and p-type semiconductors, respectively. This type of p–n heterojunction is a favourable structure for enhanced charge separation.[36] The flat band potentials are shown by the x-intercept of the linear section, which are −0.76 V, −0.72 V and 0.54 V, *vs.* RHE for TiO_2 NF, C-NW/TiO_2 NF and Cu_2O, respectively. The anodic shift of 40 mV between TiO_2 NF and C-NW/TiO_2 NF is in agreement with previous reports.[37]

The gradient of the linear portion of the plot was used to calculate the majority carrier density (N_A) calculated from eqn (3).

$$\frac{1}{C^2} = \frac{2}{\varepsilon\varepsilon_0 e N_A}\left(V - E_{fb-}\frac{k_B T}{e}\right) \quad (3)$$

where C is the capacitance, ε is the dielectric constant of TiO_2 and Cu_2O, which is 170[38] and 7.60,[39] respectively, ε_0 is the permittivity of free space, V. is the applied potential, E_{fb} is the flat band potential, e is the electron charge, k_B is the Boltzmann's constant and T is the temperature. The N_A values of Cu_2O, TiO_2 NF and TiO_2 NF/C-NWs were 5.36×10^{18} cm^{-3}, 1.06×10^{19} cm^{-3} and 1.30×10^{19} cm^{-3}, respectively. This showed that 1D TiO_2 NF had more charge carrier activity, but more studies are needed to gain conclusive results.

The valence band edge of Cu_2O, E_V, was calculated from eqn (4):

$$E_V = E_F - k_B T \ln\frac{N_V}{N_A} \quad (4)$$

where the effective density of states, $N_V = 2\left(\frac{2\pi m_h k_B T}{h^2}\right)^{\frac{3}{2}}$. The effective hole mass is denoted as $m_h = 0.58m_e$ for Cu_2O,[40] where m_e is the mass of a free electron. N_V for Cu_2O was 1.10×10^{19} cm^{-3}. The valence band edge (E_V) was 0.56 V for Cu_2O. Thus, as Cu_2O has a band gap of 2.36, the valence and conduction band positions were at 0.56 V and −1.80 V *vs.* RHE,

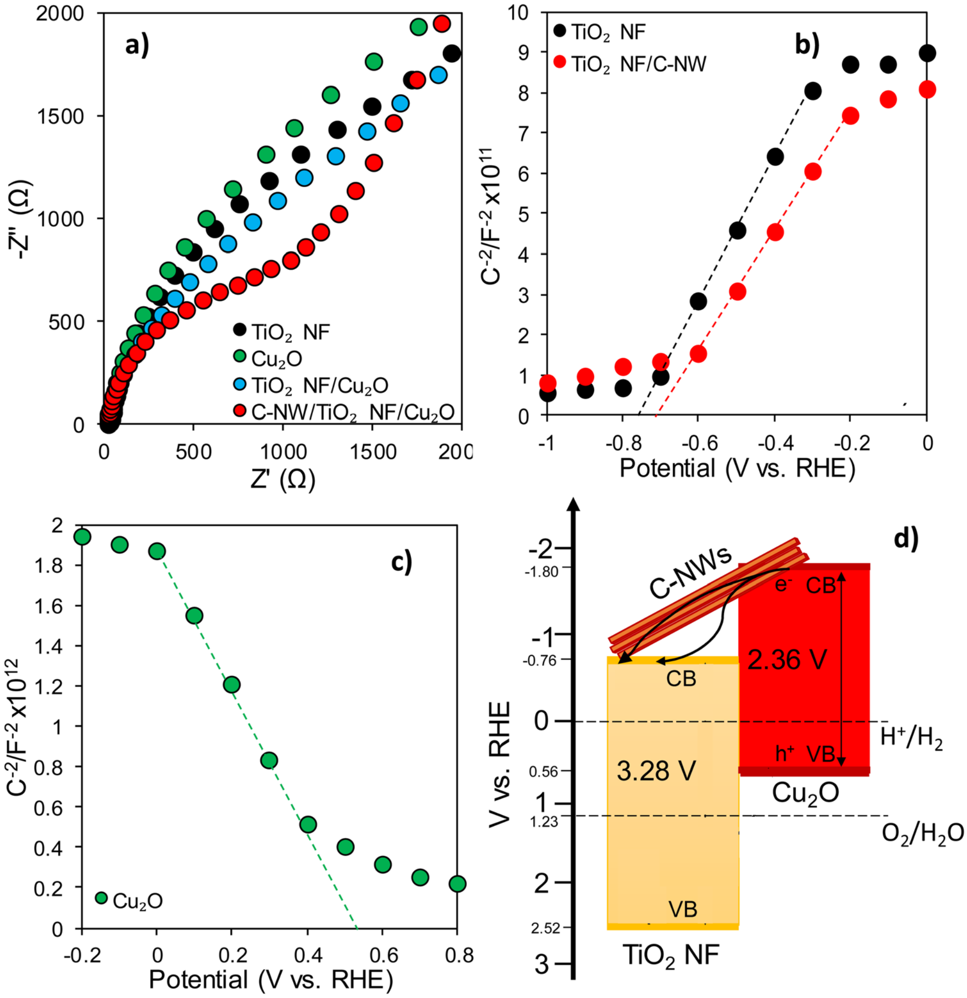

Fig. 5 (a) EIS (Nyquist plot at 0 V *vs.* RHE) of TiO_2 NF, Cu_2O, TiO_2 NF/Cu_2O and C-NW/TiO_2 NF/Cu_2O under visible light irradiation; Mott–Schottky plot of TiO_2 NF (b) and Cu_2O (c); (200 W Hg-Xe arc lamp, 0.5 M Na_2SO_4 electrolyte); (d) Schematic for the energy band structure of C-NWs/TiO_2/Cu_2O nanocomposite.

respectively. Assuming the distance between the flat band potential of TiO_2 NF and the lowest potential of the conduction band (CB) is negligible,[40] the CB of TiO_2 NF was −0.76 V *vs.* RHE. Thus, the band gap of TiO_2 NF was 3.28, so the valence band and conduction band were positioned at 2.52 V and −0.76 V *vs.* RHE, respectively.

A schematic of the energy band structure is proposed in Fig. 5d. The enhanced photoelectrochemical performance of C-NW/TiO_2 NF/Cu_2O nanocomposite was attributed to a few reasons. As Cu_2O has a narrow bandgap energy of 2.36 eV, it can be excited by visible light. The conduction band of TiO_2 lies at a more positive potential than that of Cu_2O, and the electrons from Cu_2O can inject into the conduction band of TiO_2. This prevents the recombination of photogenerated electrons and holes in Cu_2O.[41] Accumulated electrons in the conduction band of TiO_2 can then transfer to the glassy carbon electrode.[42] The addition of C-NWs further broadens the solar absorption to the visible light region. Also, the impedance spectra show that the C-NW/TiO_2 NF/Cu_2O nanocomposite has improved charge carrier density and least charge transfer resistance compared to bare TiO_2 NF and Cu_2O. This suggests that the efficient charge transfer was further assisted by the increased conductivity with C-NWs. The addition of C-NWs improved the charge carrier density; so it is proposed that the C-NWs promote electron transfer between CB of Cu_2O and CB of TiO_2, enhancing the separation of photogenerated electron-hole pairs. Overall, the introduction of C-NWs in the nanocomposite of C-NWs/TiO_2/Cu_2O enhances the PEC performance, increases charge transport, and the nanocomposite increases photostability and extends the light absorption region.

4. Conclusions

In summary, we fabricated a C-NW/TiO_2 NF/Cu_2O heterojunction nanocomposite *via* a hydrothermal treatment and subsequent solution phase method, which provided an intimate contact between 1D TiO_2 NF and Cu_2O nanocubes surrounded by C-NWs. The carbon content in the prepared samples was confirmed by both TGA and Raman spectroscopy, and DRUVS indicated that C-NWs have strong absorption properties as there was superior absorption at higher wavelengths. C-NW/TiO_2 NF/Cu_2O recorded enhanced PEC activity with higher photocurrent density, and impedance spectra illustrated less charge transfer resistance than bare TiO_2 NF and Cu_2O. After calculating the charge carrier densities of TiO_2 NF and C-NW/TiO_2 NF, it was shown that the addition of C-NWs improved the charge carrier density by promoting electron transfer. Therefore, C-NW/TiO_2 NF/Cu_2O provided superior light absorption properties, efficient charge transfer, separation of electron–hole pairs and the integration of C-NWs, which promote further electron transport within the heterojunction nanocomposite. All these properties contribute towards fabricating a nanocomposite with superior PEC activity. This work is an example of designing and fabricating effective heterojunction nanocomposite materials for solar water splitting.

Conflicts of interest

There are no conflicts of interest to declare.

Acknowledgements

This research was supported by the European Commission H2020 Marie S Curie Research and Innovation Staff Exchange (RISE) award (Grant No. 871998).

References

1 S. Li, C. Wang, M. Cai, F. Yang, Y. Liu, J. Chen, P. Zhang, X. Li and X. Chen, Facile fabrication of TaON/Bi_2MoO_6 core–shell S-scheme heterojunction nanofibers for boosting visible-light catalytic levofloxacin degradation and Cr(VI) reduction, *Chem. Eng. J.*, 2022, **428**, 131158, DOI: **10.1016/j.cej.2021.131158**.
2 S. Li, J. Chen, S. Hu, H. Wang, W. Jiang and X. Chen, Facile construction of novel Bi_2WO_6/Ta_3N_5 Z-scheme heterojunction nanofibers for efficient degradation of harmful pharmaceutical pollutants, *Chem. Eng. J.*, 2020, **402**, 126165, DOI: **10.1016/j.cej.2020.126165**.
3 C. Wang, S. Li, M. Cai, R. Yan, K. Dong, J. Zhang and Y. Liu, Rationally designed tetra (4-carboxyphenyl) porphyrin/graphene quantum dots/bismuth molybdate Z-scheme heterojunction for tetracycline degradation and Cr(VI) reduction: Performance, mechanism, intermediate toxicity appraisement, *J. Colloid Interface Sci.*, 2022, **619**, 307–321, DOI: **10.1016/j.jcis.2022.03.075**.
4 S. Li, C. Wang, Y. Liu, M. Cai, Y. Wang, H. Zhang, Y. Guo, W. Zhao, Z. Wang and X. Chen, Photocatalytic degradation of tetracycline antibiotic by a novel $Bi_2Sn_2O_7/Bi_2MoO_6$ S-scheme heterojunction: Performance, mechanism insight and toxicity assessment, *Chem. Eng. J.*, 2022, **429**, 132519, DOI: **10.1016/j.cej.2021.132519**.
5 S. Li, C. Wang, M. Cai, Y. Liu, K. Dong and J. Zhang, Designing oxygen vacancy mediated bismuth molybdate (Bi_2MoO_6)/N-rich carbon nitride (C_3N_5) S-scheme heterojunctions for boosted photocatalytic removal of tetracycline antibiotic and Cr(VI): Intermediate toxicity and mechanism insight, *J. Colloid Interface Sci.*, 2022, **624**, 219–232, DOI: **10.1016/j.jcis.2022.05.151**.
6 S. Li, M. Cai, Y. Liu, J. Zhang, C. Wang, S. Zang, Y. Li, P. Zhang and X. Li, In situ construction of a C_3N_5 nanosheet/Bi_2WO_6 nanodot S-scheme heterojunction with enhanced structural defects for the efficient photocatalytic removal of tetracycline and Cr(VI), *Inorg. Chem. Front.*, 2022, **9**, 2479–2497, DOI: **10.1039/D2QI00317A**.
7 C. Wang, M. Cai, Y. Liu, F. Yang, H. Zhang, J. Liu and S. Li, Facile construction of novel organic–inorganic tetra (4-carboxyphenyl) porphyrin/Bi_2MoO_6 heterojunction for tetracycline degradation: Performance, degradation pathways, intermediate toxicity analysis and mechanism insight, *J. Colloid Interface Sci.*, 2022, **605**, 727–740, DOI: **10.1016/j.jcis.2021.07.137**.
8 J. Luo, P. Lin, P. Zheng, X. Zhou, X. Ning, L. Zhan, Z. Wu, X. Liu and X. Zhou, In suit constructing S-scheme FeOOH/$MgIn_2S_4$ heterojunction with boosted interfacial charge separation and redox activity for efficiently eliminating antibiotic pollutant, *Chemosphere*, 2022, **298**, 134297, DOI: **10.1016/j.chemosphere.2022.134297**.
9 J. Luo, X. Zhou, F. Yang, X. Ning, L. Zhan, Z. Wu and X. Zhou, Generating a captivating S-scheme $CuBi_2O_4/CoV_2O_6$ heterojunction with boosted charge spatial separation for efficiently removing tetracycline antibiotic from wastewater, *J. Clean. Prod.*, 2022, **357**, 131992, DOI: **10.1016/j.jclepro.2022.131992**.
10 J. Luo, J. Chen, X. Chen, X. Ning, L. Zhan and X. Zhou, Construction of cerium oxide nanoparticles immobilized on the surface of zinc vanadate nanoflowers for accelerated photocatalytic degradation of tetracycline under visible light irradiation, *J. Colloid Interface Sci.*, 2021, **587**, 831–844, DOI: **10.1016/j.jcis.2020.11.044**.
11 A. L. Linsebigler, G. Lu and J. T. Yates, Photocatalysis on TiO_2 Surfaces: Principles, Mechanisms, and Selected Results, *Chem. Rev.*, 1995, **95**, 735–758, DOI: **10.1021/cr00035a013**.
12 Ü. Özgür, Y. I. Alivov, C. Liu, A. Teke, M. A. Reshchikov, S. Doğan, V. Avrutin, S.-J. Cho and H. Morkoç, A comprehensive review of ZnO materials and devices, *J. Appl. Phys.*, 2005, **98**, 041301, DOI: **10.1063/1.1992666**.
13 K. Sivula, F. Le Formal and M. Grätzel, Solar Water Splitting: Progress Using Hematite (α-Fe_2O_3) Photoelectrodes, *ChemSusChem*, 2011, **4**, 432–449, DOI: **10.1002/cssc.201000416**.
14 A. Kudo, K. Omori and H. Kato, A Novel Aqueous Process for Preparation of Crystal Form-Controlled and Highly Crystalline $BiVO_4$ Powder from Layered Vanadates at Room Temperature and Its Photocatalytic and Photophysical Properties, *J. Am. Chem. Soc.*, 1999, **121**, 11459–11467, DOI: **10.1021/ja992541y**.
15 M. Ni, M. K. H. Leung, D. Y. C. Leung and K. Sumathy, A review and recent developments in photocatalytic water-splitting using TiO_2 for hydrogen production, *Renew. Sustain. Energy Rev.*, 2007, **11**, 401–425, DOI: **10.1016/j.rser.2005.01.009**.

16 R. Abe, Recent progress on photocatalytic and photoelectrochemical water splitting under visible light irradiation, *J. Photochem. Photobiol., C*, 2010, **11**, 179–209, DOI: **10.1016/j.jphotochemrev.2011.02.003**.
17 M. Hara, T. Kondo, M. Komoda, S. Ikeda, J. N. Kondo, K. Domen, M. Hara, K. Shinohara and A. Tanaka, Cu_2O as a photocatalyst for overall water splitting under visible light irradiation, *Chem. Commun.*, 1998, 357–358, DOI: **10.1039/a707440i**.
18 S. J. A. Moniz, S. A. Shevlin, D. J. Martin, Z.-X. Guo and J. Tang, Visible-light driven heterojunction photocatalysts for water splitting – a critical review, *Energy Environ. Sci.*, 2015, **8**, 731–759, DOI: **10.1039/C4EE03271C**.
19 K. Sekar, C. Chuaicham, B. Vellaichamy, W. Li, W. Zhuang, X. Lu, B. Ohtani and K. Sasaki, Cubic Cu_2O nanoparticles decorated on TiO_2 nanofiber heterostructure as an excellent synergistic photocatalyst for H_2 production and sulfamethoxazole degradation, *Appl. Catal. B Environ.*, 2021, **294**, 120221, DOI: **10.1016/j.apcatb.2021.120221**.
20 K. Woan, G. Pyrgiotakis and W. Sigmund, Photocatalytic Carbon-Nanotube-TiO_2 Composites, *Adv. Mater.*, 2009, **21**, 2233–2239, DOI: **10.1002/adma.200802738**.
21 W. Li, Y. Bai, C. Liu, Z. Yang, X. Feng, X. Lu, N. K. van der Laak and K.-Y. Chan, Highly Thermal Stable and Highly Crystalline Anatase TiO_2 for Photocatalysis, *Environ. Sci. Technol.*, 2009, **43**, 5423–5428, DOI: **10.1021/es8037005**.
22 W. Li, Y. Bai, W. Liu, C. Liu, Z. Yang, X. Feng, X. Lu and K.-Y. Chan, Single-crystalline and reactive facets exposed anatase TiO_2 nanofibers with enhanced photocatalytic properties, *J. Mater. Chem.*, 2011, **21**, 6718, DOI: **10.1039/c1jm10115c**.
23 S. Karthikeyan, S. Kumar, L. J. Durndell, M. A. Isaacs, C. M. A. Parlett, B. Coulson, R. E. Douthwaite, Z. Jiang, K. Wilson and A. F. Lee, Size-Dependent Visible Light Photocatalytic Performance of Cu_2O Nanocubes, *ChemCatChem*, 2018, **10**, 3554–3563, DOI: **10.1002/cctc.201800439**.
24 M. Amjad, M. Iqbal, A. Faisal, A. M. Junjua, I. Hussain, S. Z. Hussain, H. A. Ghramh, K. A. Khan and H. A. Janjua, Hydrothermal synthesis of carbon nanodots from bovine gelatin and PHM3 microalgae strain for anticancer and bioimaging applications, *Nanoscale Adv.*, 2019, **1**, 2924–2936, DOI: **10.1039/C9NA00164F**.
25 Q. Cui, F. He, X. Wang, B. Xia and L. Li, Gold Nanoflower@Gelatin Core–Shell Nanoparticles Loaded with Conjugated Polymer Applied for Cellular Imaging, *ACS Appl. Mater. Interfaces*, 2013, **5**, 213–219, DOI: **10.1021/am302589g**.
26 Q. Liang, W. Ma, Y. Shi, Z. Li and X. Yang, Easy synthesis of highly fluorescent carbon quantum dots from gelatin and their luminescent properties and applications, *Carbon N. Y*, 2013, **60**, 421–428, DOI: **10.1016/j.carbon.2013.04.055**.
27 H. G. Yang, G. Liu, S. Z. Qiao, C. H. Sun, Y. G. Jin, S. C. Smith, J. Zou, H. M. Cheng and G. Q. Lu, Solvothermal Synthesis and Photoreactivity of Anatase TiO_2 Nanosheets with Dominant {001} Facets, *J. Am. Chem. Soc.*, 2009, **131**, 4078–4083, DOI: **10.1021/ja808790p**.
28 S. Sun, X. Zhang, X. Song, S. Liang, L. Wang and Z. Yang, Bottom-up assembly of hierarchical Cu_2O nanospheres: controllable synthesis, formation mechanism and enhanced photochemical activities, *CrystEngComm*, 2012, **14**, 3545, DOI: **10.1039/c2ce25071c**.
29 S. Zhang, H. Liu, C. Sun, P. Liu, L. Li, Z. Yang, X. Feng, F. Huo and X. Lu, CuO/Cu_2O porous composites: shape and composition controllable fabrication inherited from metal organic frameworks and further application in CO oxidation, *J. Mater. Chem. A*, 2015, **3**, 5294–5298, DOI: **10.1039/C5TA00249D**.
30 M. Hiramatsu and M. Hori, *Carbon Nanowalls: Synthesis and Emerging Applications*, Springer Vienna, Vienna, 2010, DOI: **10.1007/978-3-211-99718-5**.
31 F. Meng, J. Li, S. K. Cushing, J. Bright, M. Zhi, J. D. Rowley, Z. Hong, A. Manivannan, A. D. Bristow and N. Wu, Photocatalytic Water Oxidation by Hematite/Reduced Graphene Oxide Composites, *ACS Catal.*, 2013, **3**, 746–751, DOI: **10.1021/cs300740e**.
32 J. Zhang, W. Liu, X. Wang, X. Wang, B. Hu and H. Liu, Enhanced decoloration activity by $Cu_2O@TiO_2$ nanobelts heterostructures via a strong adsorption-weak photodegradation process, *Appl. Surf. Sci.*, 2013, **282**, 84–91, DOI: **10.1016/j.apsusc.2013.05.054**.
33 Y. Bessekhouad, D. Robert and J.-V. Weber, Photocatalytic activity of Cu_2O/TiO_2, Bi_2O_3/TiO_2 and $ZnMn_2O_4/TiO_2$ heterojunctions, *Catal. Today*, 2005, **101**, 315–321, DOI: **10.1016/j.cattod.2005.03.038**.
34 S. G. Babu, R. Vinoth, D. Praveen Kumar, M. V. Shankar, H.-L. Chou, K. Vinodgopal and B. Neppolian, Influence of electron storing, transferring and shuttling assets of reduced graphene oxide at the interfacial copper doped TiO_2 p–n heterojunction for increased hydrogen production, *Nanoscale*, 2015, **7**, 7849–7857, DOI: **10.1039/C5NR00504C**.
35 J. Hou, C. Yang, H. Cheng, S. Jiao, O. Takeda and H. Zhu, High-performance p-Cu_2O/n-TaON heterojunction nanorod photoanodes passivated with an ultrathin carbon sheath for photoelectrochemical water splitting, *Energy Environ. Sci.*, 2014, **7**, 3758–3768, DOI: **10.1039/C4EE02403F**.
36 S. Li, C. Wang, Y. Liu, B. Xue, W. Jiang, Y. Liu, L. Mo and X. Chen, Photocatalytic degradation of antibiotics using a novel $Ag/Ag_2S/Bi_2MoO_6$ plasmonic p–n heterojunction photocatalyst: Mineralization activity, degradation pathways and boosted charge separation mechanism, *Chem. Eng. J.*, 2021, **415**, 128991, DOI: **10.1016/j.cej.2021.128991**.
37 S. Sakthivel and H. Kisch, Daylight Photocatalysis by Carbon-Modified Titanium Dioxide, *Angew. Chem., Int. Ed.*, 2003, **42**, 4908–4911, DOI: **10.1002/anie.200351577**.
38 R. A. Parker, Static Dielectric Constant of Rutile (TiO_2), 1.6—106 K, *Phys. Rev.*, 1961, **124**, 1719–1722, DOI: **10.1103/PhysRev.124.1719**.
39 Z. Zhang and P. Wang, Highly stable copper oxide composite as an effective photocathode for water splitting via a facile electrochemical synthesis strategy, *J. Mater. Chem.*, 2012, **22**, 2456–2464, DOI: **10.1039/C1JM14478B**.
40 A. Paracchino, J. C. Brauer, J.-E. Moser, E. Thimsen and M. Graetzel, Synthesis and Characterization of

High-Photoactivity Electrodeposited Cu_2O Solar Absorber by Photoelectrochemistry and Ultrafast Spectroscopy, *J. Phys. Chem. C.*, 2012, **116**, 7341–7350, DOI: **10.1021/jp301176y**.

41 M. Wang, L. Sun, Z. Lin, J. Cai, K. Xie and C. Lin, p–n Heterojunction photoelectrodes composed of Cu_2O-loaded TiO_2 nanotube arrays with enhanced photoelectrochemical and photoelectrocatalytic activities, *Energy Environ. Sci.*, 2013, **6**, 1211, DOI: **10.1039/c3ee24162a**.

42 Y. Hou, X. Y. Li, Q. D. Zhao, X. Quan and G. H. Chen, Fabrication of Cu_2O/TiO_2 nanotube heterojunction arrays and investigation of its photoelectrochemical behavior, *Appl. Phys. Lett.*, 2009, **95**, 093108, DOI: **10.1063/1.3224181**.